ARTICLE NO. 78-1189R

Overlaid Viscous/Inviscid Model for the Prediction of Near-Field Jet Entrainment

S.M. Dash*
Aeronautical Research Associates of Princeton, Inc., Princeton, N.J.
R.G. Wilmoth†
NASA Langley Research Center, Hampton, Va.
and
H.S. Pergament‡
Aeronautical Research Associates of Princeton, Inc., Princeton, N.J.

The development of a computational model (BOAT) for calculating near-field jet entrainment, and its application to the prediction of nozzle boattail pressures, is discussed. BOAT accounts for the detailed turbulence and thermochemical processes occurring in the near-field shear layers of exhaust plumes, while interfacing with the inviscid exhaust and external flowfield regions in an overlaid, interactive manner. The ability of the model to analyze basic free shear flows is assessed by detailed comparisons with fundamental laboratory data. The overlaid methodology and the entrainment correction employed to yield effective plume boundary conditions are assessed via application of BOAT in conjunction with the codes comprising the NASA/LRC patched viscous/inviscid model for determining nozzle boattail drag for subsonic/transonic external flows. Comparisons between the predictions and data on underexpanded laboratory cold airjets are presented.

Nomenclature

$C_{D,\beta}$ = afterbody (pressure) drag coefficient
C_p = afterbody pressure coefficient, $C_p = (p-p_e)/\frac{1}{2}\rho_e u_e^2$
c_p = specific heat
F_i = X_i/W
h_i = enthalpy of ith species
k = turbulent kinetic energy
l = length scale for Prandtl mixing length model
Le = turbulent Lewis number
M = Mach number
p = pressure
P = turbulence production
Pr = turbulent Prandtl number
r = radial distance from axis
r_{eff} = radial distance to effective inviscid boundary
r_j = nozzle exit radius
T = static temperature
u = axial velocity
v = radial velocity
v_j = injection velocity
$\dot{w}_i$ = net rate of production of the ith species
x = axial distance
X_i = mole fraction of ith species
γ = ratio of specific heats
δ = boundary-layer or mixing layer thickness
δ^* = displacement thickness
ϵ = turbulent dissipation rate
μ_t = turbulent viscosity
ρ = density
σ = shear layer spreading parameter
σ_0 = spreading parameter for $u_2/u_1 = 0$
σ_k = Prandtl number of turbulent kinetic energy
σ_ϵ = Prandtl number for turbulent dissipation
ψ = stream function

Subscripts

e,E = external flow
i = ith species
I = inner stream
j,J = exhaust flow
1 = inner mixing layer boundary
2 = outer mixing layer boundary

Received July 5, 1978; presented as Paper 78-1189 at the AIAA 11th Fluid and Plasma Dynamics Conference, Seattle, Wash., July 10-12, 1978; revision received April 2, 1979.

Index categories: Jets, Wakes, and Viscous/Inviscid Flow Interactions; Computational Methods.

*Consultant. Member AIAA.
†Aerospace Engineer.
‡Senior Consultant.

Introduction

THE accurate prediction of nozzle afterbody drag requires a detailed description of the coupled viscous/inviscid flow processes occurring along the nozzle afterbody and in the near-field mixing layer growing along the plume interface, which separates the supersonic nozzle exhaust and subsonic/transonic external airstreams (Fig. 1). While analyses based upon solving the turbulent Navier-Stokes equations can provide a description of this complex flowfield, the widely disparate length scales and flow characteristics in the various regions involved lead to rather prohibitive computer time requirements in achieving results of adequate resolution. A more efficient procedure is that provided by a "patched" viscous/inviscid methodology, where each region is separately analyzed by computational procedures specifically catered to the flow processes and length scales occurring within that region. The overall flowfield solution is arrived at by patching these regional solutions together in an iterative manner. Such a patched methodology has been implemented at NASA/LRC[1-3] for subsonic/transonic external flows. For nonseparated afterbody flows, the LRC system included the relaxation procedure of South and Jameson[4] for analyzing the inviscid subsonic/transonic external flow, the supersonic exhaust plume model of Salas,[5] and an extended version of

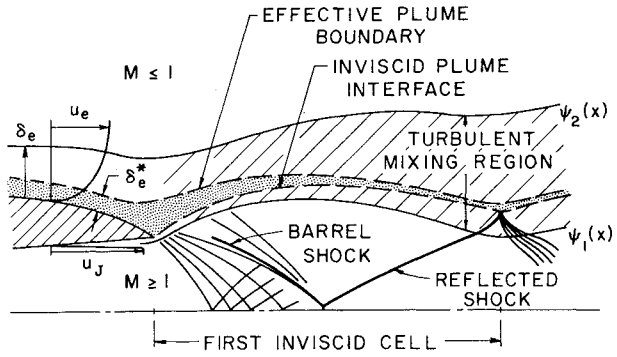

Fig. 1 Schematic of afterbody/jet exhaust flowfield.

the Reshotko-Tucker[6] turbulent boundary-layer integral method. In calculating afterbody pressures with the LRC system, the inviscid plume interface was treated as a solid surface. This procedure yielded results that substantially underpredicted the afterbody drag, because the effect of jet entrainment due to mixing processes along the interface was not accounted for. This paper presents a computational model (BOAT) which predicts near-field jet entrainment within the framework of the patched LRC system.

The computational parabolic mixing model, BOAT, contains the following features:

1) It analyzes mixing and thermochemical processes in the curved shear layer growing along the plume interface.

2) It accounts for the nonsimilar mixing associated with initial boundary layers by the inclusion of detailed turbulence model formulations and by a computational grid providing adequate resolution in the low-velocity, mass defect region.

3) It interfaces with the inviscid supersonic exhaust and subsonic/transonic external streams in an overlaid manner accounting for variable pressure gradients and edge conditions in the mixing region.

Previous models for predicting jet entrainment[7,8] have been overly simplistic in their treatment of these processes.

In developing BOAT, the best features of several current mixing/afterburning models were combined to achieve rather unique computational capabilities. In this respect, BOAT employs: 1) the same generalized treatment of thermochemical processes and implicit/explicit streamline integration procedure used in the LAPP code[9] (the JANNAF standarized model for analyzing mixing/afterburning processes in low-altitude rocket exhaust plumes§); 2) the same type of shear layer discretization, grid distribution, and computational boundary growth rules used in the GENMIX[10] code; and 3) the same type of overlaid procedure for describing variable edge conditions and pressure gradients as used in the GASL system[11] for the analysis of inviscid/shock and mixing/afterburning processes in rocket exhaust plumes. These features will be discussed in subsequent sections. A more detailed discussion of various computational aspects of BOAT is presented in Ref. 12, while a description of the computer code is provided in Ref. 13.

Inclusion of Jet Entrainment Effects in a Patched Viscous/Inviscid Flowfield Model

Overview

When the analysis of the afterbody/exhaust flow is performed via a patched methodology, the separate influences of various processes can be isolated, and their contribution in establishing afterbody pressures can be assessed individually. In this context, the specific contribution of jet entrainment can be isolated by performing the external subsonic/transonic flowfield calculation with the inviscid plume interface treated as a solid boundary. Any resulting disagreement between measured and predicted pressure levels can then be attributed largely to the specific neglect of jet entrainment. Such an approach was pursued by Putnam and Abeyounis,[2] who reported a substantial underprediction of boattail drag in analyzing laboratory cold airjet data via the NASA/LRC patched methodology, neglecting jet entrainment. Comparisons of boattail drag measurements for cold airjets with those for solid plume simulators[2] have confirmed this finding. Such analytical and experimental observations established the clear-cut requirement for incorporating the effects of jet entrainment into the NASA/LRC methodology. This involves predicting the interactive coupling between the viscous and inviscid flow processes in the exhaust plume near-field. In particular, the rate of entrainment, which is directly relatable to be the mixing rate along the curved plume interface, is influenced by the nonuniform inviscid structure in the exhaust plume and external streams, while the inviscid structure is influenced by the streamline deflections induced in the entrainment process. A systematic means of modeling the interactive phenomena is thus required which incorporates the dominant physical processes in a realistic manner.

This overall objective has been met by the introduction of two relatively new concepts, namely: 1) the use of an "overlaid" procedure for calculating mixing processes along a curved plume interface with variable pressure gradients and edge conditions taken into account, and 2) the determination of a displacement thickness type of correction to the inviscid plume interface to account for the effects of jet entrainment.

Overlaid Concept

The overlaid concept is a direct extension of classical boundary-layer methodology to the analysis of axisymmetric shear layers. In boundary-layer theory, the inviscid flow pattern is first calculated followed by a boundary-layer calculation with edge conditions and pressure gradients set by the inviscid flow pattern. In the direct extension of this approach to near-field axisymmetric shear layers, the inviscid exhaust plume and external flow patterns are first determined and the shear-layer calculation is then initiated along the inviscid plume interface (see Fig. 2). Local edge conditions and pressure gradients are set in accordance with the calculated inviscid flow pattern and the rate of growth of the shear layer. This approach closely follows the methodology introduced in the patched viscous/inviscid system developed at GASL for the analysis of rocket exhaust plume flowfields.[11] An assessment of this approach for rocket plume calculations is given in the survey paper of Ref. 15.

Effective Plume Geometry Concept

The mechanism for modifying the inviscid plume geometry to account for jet entrainment is a direct extension of the weak interaction approach in standard boundary-layer (BL) theory. In BL theory, the solid wall shape is modified so that the "new" effective wall shape induces streamline deflections in the inviscid solution compatible with the viscous flow pattern. A standard modification involves applying an injection velocity boundary condition $v(x)$ along the solid wall shape, or, equivalently, adding a displacement thickness $\delta^*(x)$ to the solid wall shape (Fig. 3). For compressible boundary layers over curved surfaces (with δ^* small in comparison to the transverse extent of the body), the relationship between v and δ^* is given by:

$$\rho v = \frac{\partial}{\partial x}(\rho_e u_e \delta^*) \tag{1}$$

where x is measured along the body surface, ρ is the surface density, and δ^* is given by the standard formulation.

§A new JANNAF standarized plume model,[14] now under development at Aeronautical Research Associates of Princeton, contains an extended version of BOAT as a component part.

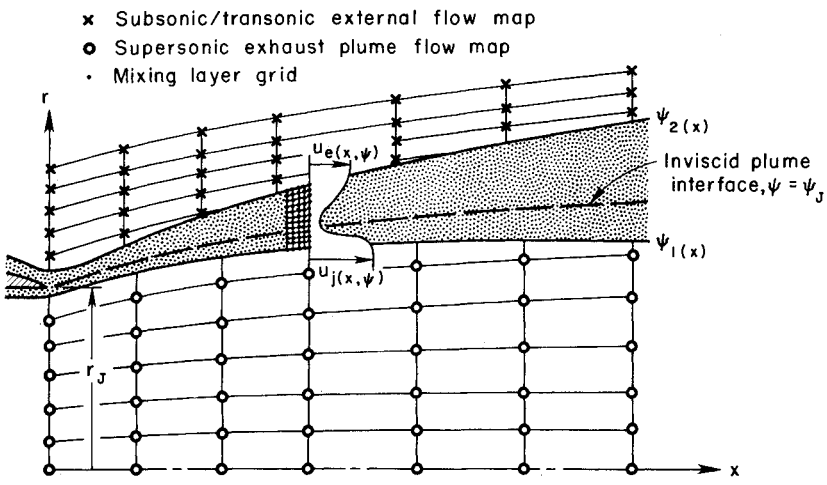

Fig. 2 Schematic of mixing layer overlaid on jet exhaust and external flow maps.

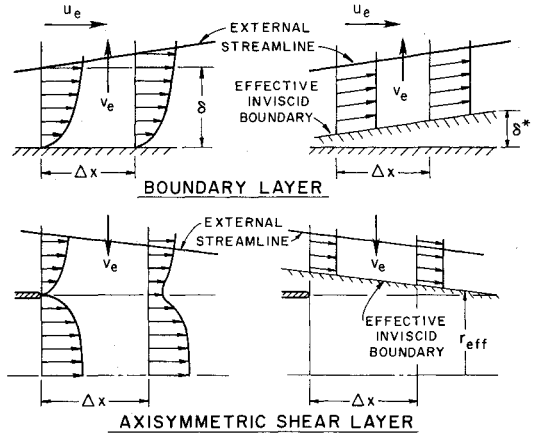

Fig. 3. Effective boundary concept.

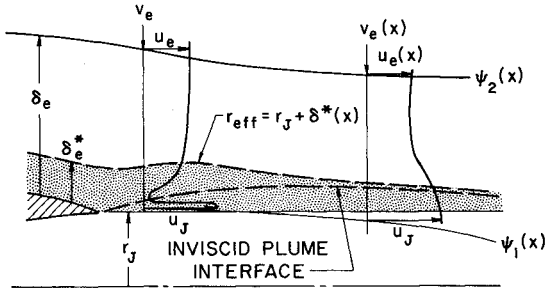

Fig. 4 Determination of effective plume boundary shape for mildly underexpanded plume with large external boundary layer.

In extending this concept to near-field jet mixing, we seek an "effective" plume geometry that will induce streamline deflections in the inviscid external flow solution compatible with those determined in the overlaid mixing calculation. Specifically, the inviscid boundary condition sought must reproduce the entrainment velocity variation $v_e(x)$ at the position of the outer shear-layer edge (Fig. 3).

For subsonic/transonic afterbody flows presently under consideration, the degree of underexpansion at the nozzle exit is moderate, while the external boundary-layer thickness is quite substantial (Fig. 4). Here, significant negative streamline deflections are induced by the mixing away of the low-velocity, mass defect region of the external boundary layer. These streamline deflections are comparable in magnitude to those induced in the external stream by the inviscid plume geometry (i.e., by the "blockage effect" due to plume underexpansion). The specific methodology used to determine the effective plume geometry for this class of problems is discussed below.

Procedure for Determining Effective Plume Geometry and Afterbody Pressures

1) A converged solution of the exhaust/external flowfield is obtained using the NASA/LRC patched methodology neglecting entrainment. This yields inviscid flowfield maps for the subsequent overlaid mixing calculation.

2) The overlaid mixing of the exhaust/external streams along the plume interface is performed, initialized by a profile containing the external boundary layer. In view of the modest degree of underexpansion, the mixing analysis is performed in standard cylindrical coordinates.¶ This yields the jet entrainment velocity distribution $v_e(x)$ along the outer boundary of the mixing region (Fig. 4), which includes contributions from both viscous (mixing) and inviscid (blockage) processes.

3) An injection velocity distribution $v_j(x)$ for the inviscid external subsonic/transonic flow is defined along the cylindrical surface $r=r_j$ (Fig. 4). If the mixing layer thickness was small in comparison with r_j, the $v_e(x)$ distribution would serve this purpose. For the thick mixing layers under consideration, $v_j(x)$ is obtained from $v_e(x)$ via the relation:

$$v_j(x) = \frac{\rho_e(x) r_e(x)}{\rho_j r_j} v_e(x) \tag{2}$$

4) An effective displacement thickness distribution, $\delta^*(x)$, is determined from the relation

$$\frac{d\delta^*(x)}{dx} + \delta^*(x) \frac{d\ell n \zeta_e u_e}{dx} = \frac{\zeta_j v_j(x)}{\zeta_e u_e(x)} \tag{3}$$

with the integration initiated at the nozzle exit plane, where δ^* is the displacement thickness of the external boundary layer. The pressure gradient term, $d\ell n \zeta_e u_e/dx$, in the preceding relation has been found to provide negligible contributions to the δ^* distribution for cases studied to date, and has not been retained in the calculations reported herein.

5) The effective plume geometry is obtained by adding the δ^* distribution to the cylindrical surface $r=r_j$. It has been demonstrated[12,16] that in solving the inviscid external flowfield over this effective geometry, the $v_e(x)$ solution is accurately reproduced. It has also been established that use of the injection boundary condition, $v_j(x)$, along the cylinder $r=r_j$ will also reproduce the $v_e(x)$ distribution.

¶Plume-oriented boundary-layer coordinates would be required for highly underexpanded plumes—see Ref. 12, 14 or 15.

6) A revised pressure distribution along the nozzle afterbody is determined by performing the inviscid subsonic/transonic flow calculation over the effective geometry comprised of the afterbody/cylinder combination plus the added $\delta^*(x)$ distribution.

For the preliminary calculations presented herein, no further iterations were performed. In the extension of this work[16]; however, further iterations were performed which required successive inviscid exhaust plume, external flow, and overlaid mixing calculations until full convergence was achieved.

Computational Procedures in the BOAT Code

Governing Equations**

BOAT solves the parabolic jet mixing equations in transformed (x,ψ) coordinates. The resultant system of equations is now listed and includes equations for the turbulent kinetic energy k and dissipation ϵ, as required in the two-equation turbulence model option.

Axial momentum:

$$\frac{\partial u}{\partial x} = -\frac{1}{\rho u}\frac{\partial p}{\partial x} + \frac{1}{\psi}\frac{\partial x}{\partial \psi}\left(A\frac{\partial u}{\partial \psi}\right) \tag{4}$$

Energy:

$$c_p\frac{\partial T}{\partial x} = \frac{1}{\rho}\frac{\partial p}{\partial x} - \frac{1}{\rho u}\sum h_i \dot{w}_i + \frac{1}{\psi}\frac{\partial}{\partial \psi}\left(\frac{c_p}{Pr}A\frac{\partial T}{\partial \psi}\right)$$

$$+\frac{A}{\psi}\left[\left(\frac{\partial u}{\partial \psi}\right)^2 + \frac{Le}{Pr}\frac{\partial}{\partial \psi}\sum_i c_{p_i}\frac{\partial F_i}{\partial \psi}\right] \tag{5}$$

Species continuity:

$$\frac{\partial F_i}{\partial x} = \frac{1}{\psi}\frac{\partial}{\partial \psi}\left(\frac{Le}{Pr}A\frac{\partial F_i}{\partial \psi}\right) + \frac{\dot{w}_i}{\rho u} \tag{6}$$

Turbulent kinetic energy:

$$\frac{\partial k}{\partial x} = \frac{1}{\psi}\frac{\partial}{\partial \psi}\left(\frac{A}{\sigma_k}\frac{\partial k}{\partial \psi}\right) + \frac{1}{u}(P-\epsilon) \tag{7}$$

Turbulent dissipation:

$$\frac{\partial \epsilon}{\partial x} = \frac{1}{\psi}\frac{\partial}{\partial \psi}\left(\frac{A}{\sigma_\epsilon}\frac{\partial \epsilon}{\partial \psi}\right) + \frac{\epsilon}{uk}(C_1 P - C_2\epsilon) \tag{8}$$

where

$$A = \mu_t\frac{\rho u r^2}{\psi}, \qquad P = \frac{Au}{\psi}\left(\frac{\partial u}{\partial \psi}\right)^2$$

and the transformation from (x,r) to (x,ψ) coordinates is given by:

$$\psi\frac{\partial \psi}{\partial r} = \rho u r, \qquad \psi\frac{\partial \psi}{\partial x} = -\rho v r \tag{9}$$

The jet entrainment velocity $v_e(x)$ is determined by inversion of the stream function transformation [Eq. (9)] at each axial station, assuming that v along the inner boundary is given by the inviscid solution.

**In extensions of BOAT to systems with significant chemical reactions, the total enthalpy is used as the dependent variable in solving the energy equation (see Ref. 14).

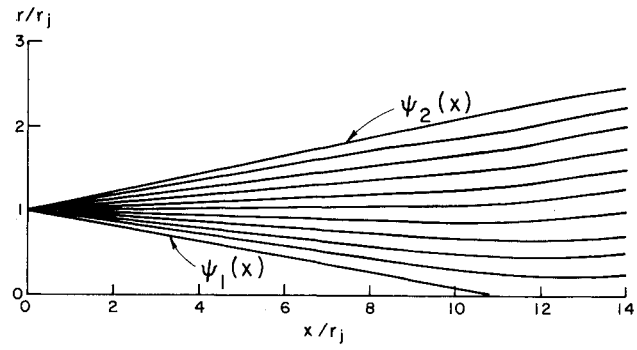

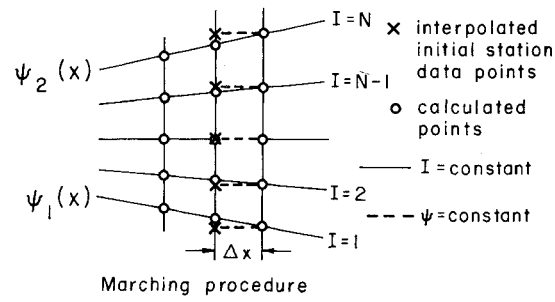

Fig. 5 Computational network in BOAT.

Computational Domain

Referring to Fig. 5, BOAT discretizes the mixing region, spanning the computational domain between $\psi_1(x)$ and $\psi_2(x)$ with a fixed number of grid intervals equally spaced in $\Delta\psi$. This is analogous to the approach employed in GENMIX.[10] However, while GENMIX integrates the flowfield equations along the lines $\omega = \text{const}\,[\omega = (\psi-\psi_1)/(\psi_2-\psi_1)]$, BOAT performs the integration along the actual streamlines. This is accomplished by extending the initial array (at both ends) to accommodate the growth of the shear layer "computationally" in the next integration step (see lower half of Fig. 5) and redistributing the grid points in equal increments of $\Delta\psi = [\psi_2(x+\Delta x) - \psi_1(x+\Delta x)]/M$, where M is the constant number of grid increments. For optimal efficiency, the redistribution is done at the stage in the program where the calculated arrays are reset into the initial arrays.

The growth of the computational boundaries, $\psi_{1,2}(x)$, is given by rules related to the local-edge gradients analogous to those introduced in GENMIX.[10] These rules differ with the turbulence model formulation (see Ref. 12), and must be such that the computational mixing boundaries grow fast enough to encompass the physical mixing region. It should be stressed that these growth rules serve only to confine the computational domain to span the region of actual mixing (for numerical efficiency) and do not influence physical mixing rates and the rate of entrainment.

Integration Procedure

The governing parabolic flowfield equations are integrated along streamlines employing the same mixed implicit/explicit formulation used in LAPP.[9] Of particular interest is the implicit treatment of the production term in the species continuity equation. The finite-difference expression for Eq. (6) (see Fig. 5) is written:

$$(F_i)_{K+1,I} = (F_i)_{K,I} + \frac{\Delta x}{\psi_I}\frac{\partial}{\partial \psi}\left(\frac{Le}{Pr}A\frac{\partial F_i}{\partial \psi}\right)_{K,I} + \frac{(\dot{w}_i)_{K+1,I}\Delta x}{(\rho u)_{K,I}} \tag{10}$$

where standard central difference expressions are used to evaluate the first and second derivatives. The species mole

fractions at station $K+1,I$ are determined by linearizing the source terms $(w_i)_{K+1,I}$, utilizing the appropriate chemical rate expression. The complete set of linearized equations for all species, $(F_i)_{K+1}$, are then solved via matrix inversion techniques. The energy, momentum, and turbulence equations are solved by a fully explicit procedure. Reference 12 gives more details on the integration procedures utilized.

The maximum allowable marching step, Δx, must satisfy explicit parabolic stability considerations. The chemistry terms impose no stability limitation on the step size due to their implicit formulation. However, to insure an accurate description of chemical processes when the chemistry is "fast" (i.e., when one or more reactions are near equilibrium), a maximum allowable temperature change $\Delta T_{\max}$ (input to the code) is permitted along a streamline in a single integration step. Should the temperature change exceed this value, the step size is repeatedly halved until the temperature change is less than $\Delta T_{\max}$.

BOAT treats the thermodynamic propeties and chemical kinetic rate expressions in a similar manner to that employed in the LAPP code.[9] Thermodynamic data are taken directly from the JANNAF tables,[17] while generalized reaction types and rate coefficient expressions are available as part of the input data, enabling the computation of the species production rates $(\dot{w}_i)$. This approach is sufficiently broad-based to permit analyzing most chemical systems of practical interest. In practice, users would build a "library" of thermodynamic and rate data and package it for various chemical systems on permanent files in a form compatible for direct input into BOAT. Applications of BOAT to chemically reacting flows are reported in Refs. 16 and 18.

Overlaid Procedure

In this procedure, detailed inviscid exhaust/external flow solutions are supplied to BOAT via arrays of $u(r)$, $p(r)$, and $T(r)$ at arbitrary axial stations. BOAT processes these data (see Ref. 12 for details) yielding orderly vector arrays of the form $\bar{V}^K_{\text{jet}}(x_I,\omega_J)$ and $\bar{V}^K_{\text{ext}}(\tilde{x}_I,\tilde{\omega}_J)$, where $\bar{V}^K=(r,u,T,p)$ in mapped stream-function (x,ω) coordinates, which eliminates the need for inviscid map-searching procedures. Referring to Fig. 2, at a given station x, the value of ψ_1 at the lower boundary is known and we desire edge conditions (u_1,T_1) and the radial location (r_1) consistent with the inviscid exhaust plume solution. Forming $\omega=\psi_I/\psi_{\text{jet}}$, these properties are readily obtained from the $\bar{V}_{\text{jet}}$ array. Similarly, knowing the value of ψ_2 at the upper boundary, upper edge properties are determined. The mismatch in the radial position r_2 between the mapped arrays and that obtained via inversion of Eq. (9), is reflective of the mass deficit/excess in the shear layer in comparison with the inviscid flow solutions. The variable pressure gradients across the shear layer are directly obtained from the mapped arrays, i.e., $p_x(x,\psi)=[\bar{V}^4(x_{I+1},\omega)-\bar{V}^4(x_I,\omega)]/(x_{I+1}-x_I)$ where $x_I<x<x_{I+1}$ and $\omega=\psi/\psi_{\text{jet}}$ for each individual streamline ψ.

Turbulence Model Description and Applications to Simple Free Shear Layer Flows

Mixing Length (ML) Model

In the extended ML model employed in BOAT, the turbulent viscosity μ_t, at all interior points, is given by the expression

$$\mu_t=\rho l^2\left|\frac{\partial u}{\partial y}\right| \tag{11a}$$

and on the axis by

$$\mu_t=\rho l^3\left|\frac{\partial^2 u}{\partial y^2}\right| \tag{11b}$$

where the mixing length l is linearly related to the characteristic thickness δ of the mixing region (i.e., $l/\delta=\text{const}$). The definitions of δ are shown in Fig. 6. The ratio of l/δ employed is 0.065 until the mixing reaches the axis and 0.080 downstream of this position.

Two-Equation Model

In the $k\epsilon 2$ model, the turbulent viscosity is given by:

$$\mu_t=C_\mu\rho(k^2/\epsilon) \tag{12}$$

where C_μ and the constants C_1, C_2, σ_k, and σ_ϵ have been extracted directly from Ref. 19. As in the ML model, the constants differ for near-field (two-dimensional) and far-field (axisymmetric) situations.

Simple Two-Dimensional Shear Layers

A fundamental check of the code/turbulence model combination has been obtained by analyzing spread rates and velocity and shear stress profiles for incompressible shear layers formed between two moving streams. Spread rates are generally defined in terms of the spreading parameter σ,

$$\sigma=\frac{1.855\Delta x}{\Delta(y_{0.1}-y_{0.9})} \tag{13}$$

where $\Delta(y_{0.1}-y_{0.9})$ is the change in the effective shear layer width over the distance Δx. The effective width is defined as the distance between the points where the nondimensional velocity ratio $\tilde{u}=(u-u_2)/(u_1-u_2)=0.1$ and 0.9. Results obtained from BOAT using both the ML and $k\epsilon 2$ turbulence models are compared with spread rates from various investigators in Fig. 7. The data were compiled and reviewed by Rodi,[20] with the relatively large spread in the data being attributed to varying turbulence levels in the freestreams. The higher values of σ (smaller spread rates) correspond to the smaller freestream turbulence levels. Since the shear layer boundary conditions in BOAT assume zero freestream turbulence, the predictions should match these higher values. Figure 7 shows that both the $k\epsilon 2$ and ML model (with $l/\delta=0.065$) predictions are in good agreement with these data. In terms of profile shapes, both the $k\epsilon 2$ and ML models adequately predict both the velocity and turbulent shear stress profiles, as illustrated in Fig. 8.

Shear Layer Formed from Initial Boundary Layers

Of particular interest for the present jet entrainment problem is the ability to accurately analyze the nonsimilar mixing region associated with a shear layer formed from initial boundary layers. Detailed data for such a situation

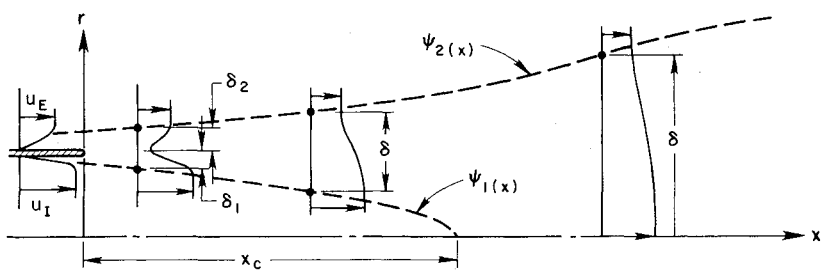

Fig. 6 Length scales in Prandtl mixing length model.

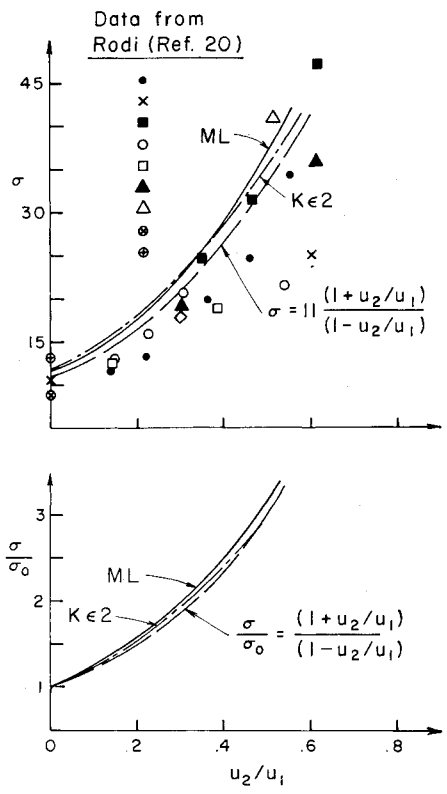

Fig. 7 Comparison between predicted and measured spread rates for two-dimensional shear layers.

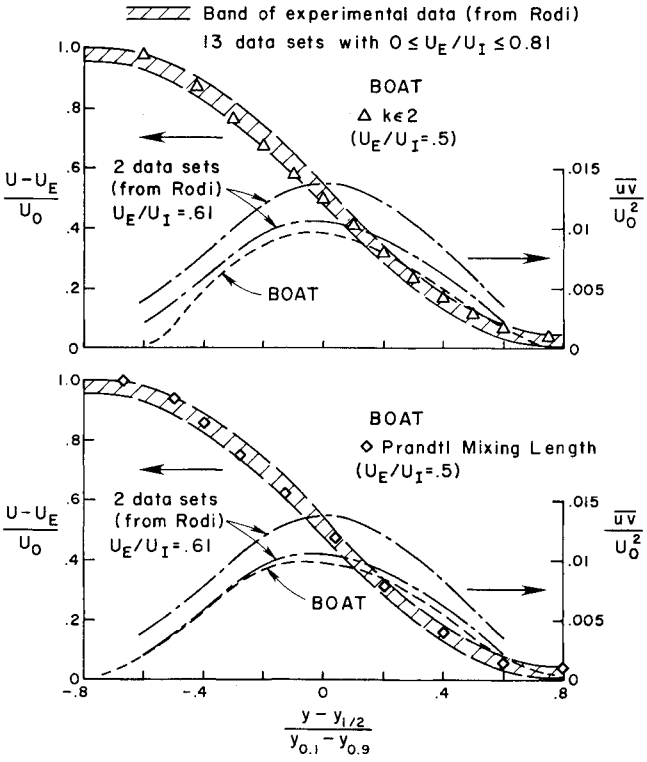

Fig. 8 Comparison between predicted and measured velocity and shear stress profiles for two-dimensional shear layers.

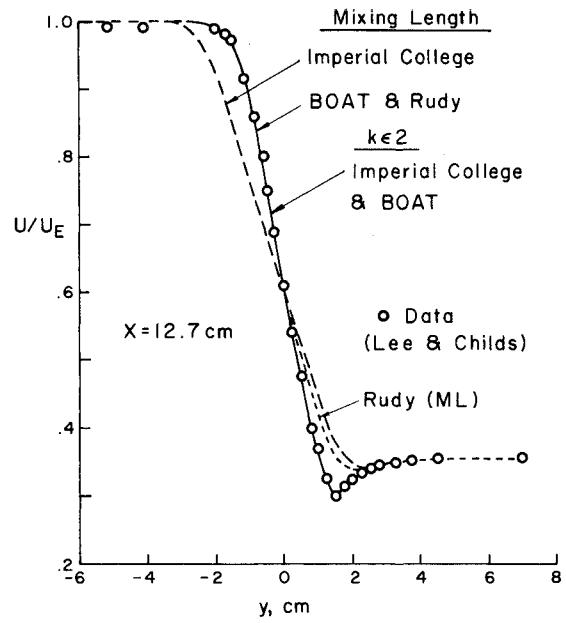

Fig. 9 Comparison between predicted and measured velocity profiles for two-dimensional shear layer with initial boundary layers.

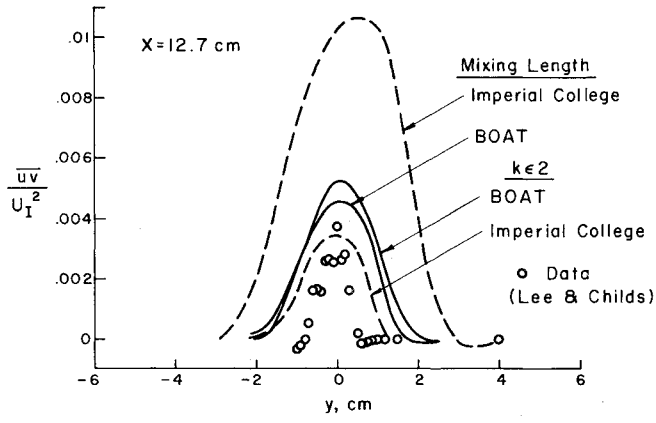

Fig. 10 Comparison between predicted and measured shear stress profiles for two-dimensional shear layer with initial boundary layers.

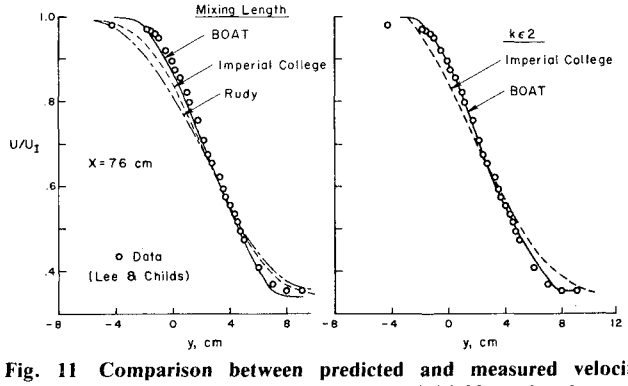

Fig. 11 Comparison between predicted and measured velocity profiles for two-dimensional shear layer with initial boundary layers.

have been provided by Lee[21] and comprise test case 4 of the NASA Free Shear Flow Conference.[22]

In Fig. 9, the predicted velocity profiles obtained with BOAT, employing both the ML (with $l/\delta = 0.065$ and the multiple length scale provision shown in Fig. 6) and $k\epsilon 2$ models, are compared with the Lee data at 12.7 cm, as well as with ML and $k\epsilon 2$ predictions by Launder et al.[19] and ML predictions by Rudy and Bushnell.[23] The BOAT ML predictions and both $k\epsilon 2$ predictions fit the data quite well. The ML predictions of both Launder and Rudy do not pick up the velocity-defect region at all. Similar trends regarding the predictive capability of each model are observed in Fig. 10, which compares predicted and measured shear stress profiles. Proceeding downstream to $x = 76$ cm (Fig. 11), where the

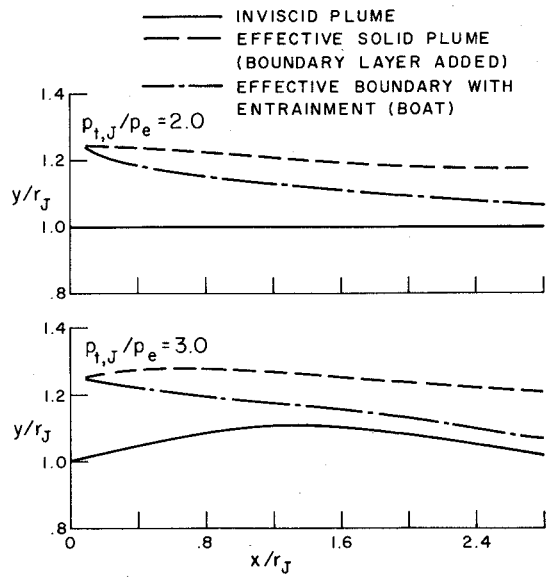

Fig. 12 Comparison between effective boundary calculated by BOAT and effective solid plume boundary for fully expanded and underexpanded jet mixing, $M_e = 0.40$, $k\epsilon 2$ turbulence model.

mixing takes on a simple shear layer type of behavior, the BOAT ML predictions are quite good in contrast to the predictions of the ML models in the other two codes. The BOAT $k\epsilon 2$ predictions are also quite good, while those in the GENMIX code are somewhat poorer.

Comparisons between Interactive Model Predictions and Experimental Data

Preliminary results have been obtained for one of the boattail nozzle configurations tested with cold airjets by Reubush.[24] Experimental boattail surface pressures are presented[24] for various freestream Mach numbers and jet total pressure ratios ($P_{t,j}/P_e$). BOAT calculations were performed for a fully expanded ($P_{t,j}/P_e = 2$) and a modestly underexpanded ($P_{t,j}/P_e = 3$) jet with a nominal velocity ratio, u_2/u_1, of about 0.5, and freestream Mach number of 0.4. Initial external boundary layers at the end of the boattail were quite thick in both cases.

Effective Plume Boundaries

The effective boundaries downstream of the nozzle exit for the two cases investigated are shown in Fig. 12 ($x/r_j = 0$ corresponds to the end of the boattail, which is also the nozzle exit). Also shown are the inviscid plume interfaces and the effective solid plume boundaries obtained by treating the inviscid plume interface as a solid body to which is added the calculated boundary-layer displacement thickness. This latter boundary has previously been used to predict jet plume blockage effects without considering entrainment.[2] The important observation here is that when the effects of entrainment are considered, the effective plume boundary is substantially reduced in size, primarily because the mass deficit, associated with the initial boundary layers, mixes away rather rapidly. Thus, treating the inviscid plume as a solid boundary is quite unrealistic. Since jet aircraft nozzles are generally located in regions of thick boundary layers (e.g., near the aft end of the aircraft), a similar reduction in effective boundary size is expected.

Predicted and Measured Boattail Pressures

Boattail pressure distributions predicted by the South and Jameson model,[4] using the effective solid plume (no entrainment) and the effective boundary (with entrainment), are compared with the experimental data in Fig. 13. A sketch of

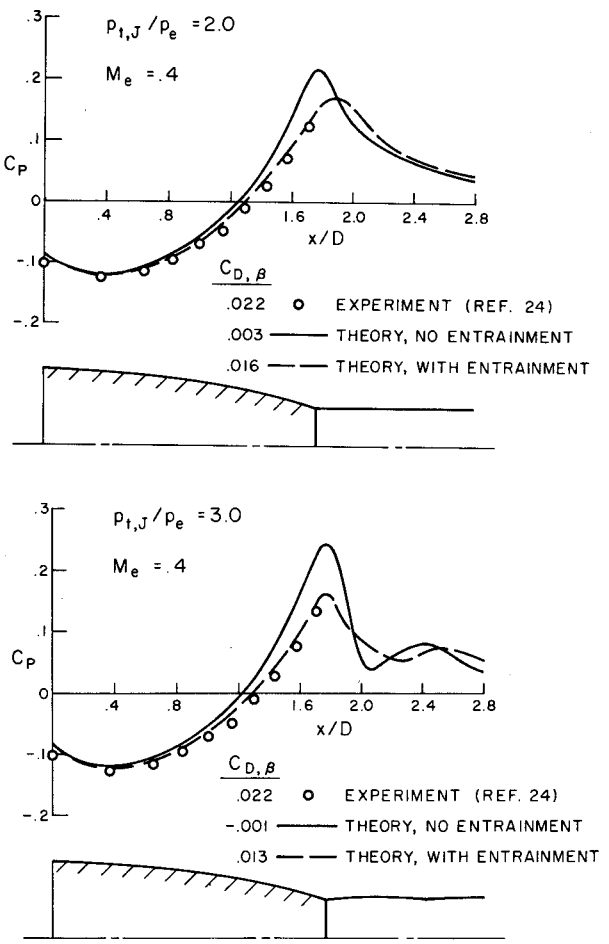

Fig. 13 Effects of jet entrainment on boattail pressure distributions and comparison with experimental data, $M_e = 0.40$, $k\epsilon 2$ turbulence model.

the boattail geometry and inviscid plume shape is also indicated. Excellent agreement with the experimental pressure distribution is obtained at both jet pressure ratios when entrainment effects are included, with a corresponding improvement in the predicted boattail drag coefficient $C_{D,\beta}$. While the effect of underexpansion on the inviscid plume geometry appears relatively small (see Fig. 12), the pressure distribution is quite sensitive to this effect, as evidenced by the variations in C_p downstream of the nozzle exit (Fig. 13). Including the (viscous) effect of entrainment decreases these variations, indicating a weakening of the effective wavelike amplitude of the inviscid plume. These limited comparisons indicate that the entrainment model appears to provide a reasonable representation of the boattail flowfield.

Sensitivity Studies

By varying some of the input and modeling parameters required for entrainment calculations, the relative dependence of the effective geometry (and hence, boattail pressures) on these parameters can be established. Areas explored were turbulence models and pressure gradients.

Sensitivity to Turbulence Models

By performing the calculations with both a simple (ML) and more detailed ($k\epsilon 2$) turbulence model, the level of sophistication required in the turbulence modeling can be assessed. Comparisons of the predicted effective boundary shape for both cases studied are given in Fig. 14. In both cases, the ML model predicts a more rapid rate of mixing (and corresponding rate of entrainment) than the $k\epsilon 2$ model and thus a narrower effective plume geometry. The difference is

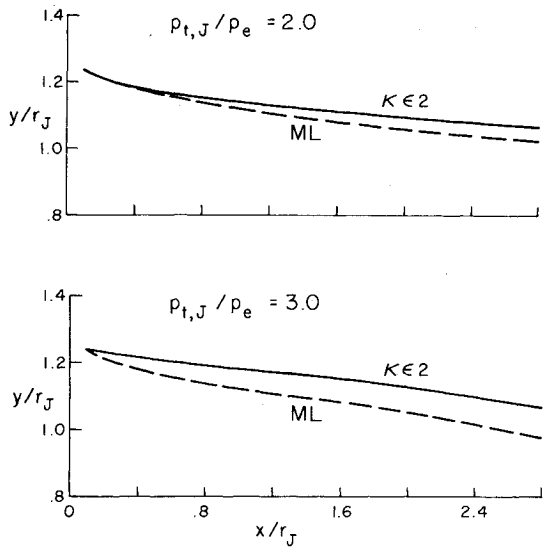

Fig. 14 Effect of turbulence model on effective plume boundary shape.

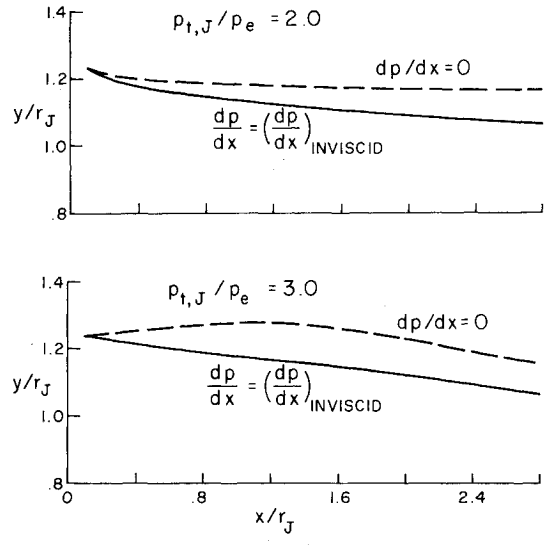

Fig. 15 Effect of pressure gradient on effective plume boundary shape, $k\epsilon 2$ turbulence model.

substantially more pronounced in the underexpanded case where pressure gradients exist and the shear layer edge conditions are varying. Inviscid calculations over these geometries, and those for other similar test cases, have indicated that either the ML or $k\epsilon 2$ model can yield a reasonable estimate of entrainment effects for fully expanded jets, while the $k\epsilon 2$ model produces better results for underexpanded jets.

Sensitivity to Pressure Gradients

To test the sensitivity of the present results to pressure gradients, BOAT calculations (with the $k\epsilon 2$ model) were repeated with the pressure gradient terms in both the momentum and energy equations set identically to zero. A comparison of the effective plume geometry with and without pressure gradients is shown in Fig. 15. With the pressure gradients deleted, the entrainment effect is markedly reduced; in fact, the effective boundary shapes are only slightly improved from those obtained treating the plume interface as a solid boundary. Clearly, the favorable near-field pressure gradients contribute strongly to accelerating the flow in the low-velocity mass deficit region and thus increase the overall entrainment rate.

Concluding Remarks

1) The use of a "displacement thickness" correction to account for the effects of jet entrainment has been demonstrated. A computational model (BOAT) has been developed which predicts the rate of jet entrainment via an overlaid, parabolic procedure from which the displacement thickness correction can be determined. Limited comparisons between predicted and measured boattail pressure distributions have been quite favorable, indicating that the use of the BOAT code, in conjunction with the patched NASA/LRC system, shows great promise as a computational approach for predicting nozzle boattail drag. This conclusion has been fortified by the systematic comparisons achieved in the extension of this methodology described in Ref. 16.

2) Sensitivity studies have indicated that the $k\epsilon 2$ model, which accounts for the turbulence "history," yields overall results of better quality than the ML model for underexpanded, variable pressure plumes. The assessment (in BOAT) of various turbulence models at higher Mach numbers and for reacting/high-temperature exhausts via comparisons with a broad-based body of data (supersonic jets/shear layers, turbulent diffusion flames, rocket exhaust plume data, etc.) is reported in Ref. 18.

3) The pressure changes produced by the entrainment correction suggest that the weak viscous/inviscid interaction approach adopted for this study is adequate. The rather large influence of pressure gradients on the entrainment rate clearly demonstrates the inadequacy of isobaric mixing assumptions employed in earlier modeling efforts.[7,8] Further studies are in progress to assess the adequacy of the viscous-inviscid coupling procedure over a wider range of operating conditions, some of which are reported in Ref. 16.

Acknowledgments

This effort was supported by NASA Langley Research Center under Contract NAS1-14794, and monitored by R.G. Wilmoth.

References

[1] Reubush, D.E. and Putnam, L.E., "An Experimental and Analytical Investigation of the Effect on Isolated Boattail Drag of Varying Reynolds Number up to 130×10^6," NASA TN D-8210, May 1976.

[2] Putnam, L.E. and Abeyounis, W.K., "Experimental and Theoretical Study of Flow Fields Surrounding Boattail Nozzles at Subsonic Speeds," AIAA Paper 76-675, Palo Alto, Calif., July 1976.

[3] Wilmoth, R.G., "Analytical Study of Viscous Effects on Transonic Flow over Boattail Nozzles," AIAA Paper 77-223, Los Angeles, Calif., Jan. 1977.

[4] South Jr., J.D. and Jameson, A., "Relaxation Solutions for Inviscid Axisymmetric Transonic Flow over Blunt or Pointed Bodies," *Proceedings of the AIAA Computational Fluid Dynamics Conference*, July 1973, Palm Springs, Calif., pp. 8-17.

[5] Salas, M.D., "The Numerical Calculation of Inviscid Plume Flow Fields," AIAA Paper 74-523, Palo Alto, Calif., June 1974.

[6] Reshotko, E. and Tucker, M., "Approximate Calculation of the Compressible Turbulent Boundary Layer with Heat Transfer and Arbitrary Pressure Gradient," NASA TN 4154, 1957.

[7] Yaros, S.F., "An Analysis of Transonic Viscous/Inviscid Interactions on Axisymmetric Bodies with Solid Stings or Real Plumes," Ph.D. Dissertation, University of Tennessee, 1977.

[8] Grossman, B. and Melnik, R., "The Numerical Computation of the Transonic Flow Over Afterbodies Including the Effect of Jet-Plume and Viscous Interactions," AIAA Paper 75-62, Pasadena, Calif., Jan. 1975.

[9] Mikatarian, R.R., Kau, C.J., and Pergament, H.S., "A Fast Computer Program for Nonequilibrium Rocket Plume Predictions," AFRPL-TR-72-94, Aug. 1972.

[10] Patankar, S.W. and Spalding, D.B., *Heat and Mass Transfer in Boundary Layers*, 2nd ed., Intertext Books, London, 1970.

[11] Dash, S., Boccio, J., and Weilerstein, G., "A Computational System for the Prediction of Low Altitude Rocket Plume Flowfields: Vol. I—Integrated System; Vol. II—Inviscid Plume Model (MAXIPLUM); Vol. III—Mixing/Afterburning Model (CHEMX),"

GASL TR-239, General Applied Science Laboratories, Inc., Westbury, N.Y., Dec. 1976.

[12] Dash, S.M. and Pergament, H.S., "A Computational Model for the Prediction of Jet Entrainment in the Vicinity of Nozzle Boattails," NASA CR 3075, Dec. 1978.

[13] Dash, S.M. and Pergament, H.S., "The BOAT Code Program Users Manual," NASA CR 159001, Nov. 1978.

[14] Dash, S.M., Pergament, H.S., and Thorpe, R.D., "A Modular Approach for the Coupling of Viscous and Inviscid Processes in Exhaust Plume Flows," AIAA Paper 79-0150, New Orleans, La., Jan. 1979.

[15] Dash, S.M. and Pergament, H.S., "The Analysis of Low Altitude Rocket and Aircraft Plume Flowfields: Modeling Requirements and Procedures," *Proceedings of the JANNAF 10th Plume Technology Meeting,* CPIA Pub. 291, Vol. I, 1977, pp. 53-132.

[16] Wilmoth, R.G., Dash, S.M., and Pergament, H.S., "A Numerical Study of Jet Entrainment Effects on the Subsonic Flow Over Nozzle Afterbodies," AIAA Paper 79-0135, New Orleans, La., Jan. 1979.

[17] *JANNAF Thermochemical Tables,* 2nd ed., NBS-NSRDS No. 37, National Bureau of Standards, Washington, D.C., 1971.

[18] Pergament, H.S., Dash, S.M., and Varma, A.K., "Evaluation of Turbulence Models for Rocket and Aircraft Plume Flowfield Predictions," AIAA Paper 79-0359, New Orleans, La., Jan. 1979.

[19] Launder, B.E., et al., "Prediction of Free Shear Flows: A Comparison of Six Turbulence Models," *Free Turbulent Shear Flows,* Vol. I, NASA SP-321, July 1972, pp. 361-426.

[20] Rodi, W., "A Review of Experimental Data of Uniform Density Free Turbulent Boundary Layers," *Studies in Convection,* Vol. I, edited by B.E. Launder, Academic Press, London, 1975, pp. 79-166.

[21] Lee, S.L., "A Study of the Two-Dimensional Free Turbulent Mixing Between Converging Streams With Initial Boundary Layers," Ph.D. Dissertation, University of Washington, 1966.

[22] Anon., *Free Turbulent Shear Flows,* Vols. I and II, NASA SP-321, July 1972.

[23] Rudy, D.H. and Bushnell, D.M., "A Rational Approach to the Use of Prandtl's Mixing Length Model in Free Turbulent Shear Flow Calculations," *Free Turbulent Shear Flows,* Vol. I, NASA SP-321, July 1972, pp. 67-138.

[24] Reubush, D.E., "Experimental Study of the Effectiveness of Cylindrical Plume Simulators for Predicting Jet-On Boattail Drag at Mach Numbers up to 1.30," NASA TN D-7795, 1974.